JACS Au
AN OPEN ACCESS JOURNAL OF THE AMERICAN CHEMICAL SOCIETY

pubs.acs.org/jacsau

Article

In Situ Multinuclear Magic-Angle Spinning NMR: Monitoring Crystallization of Molecular Sieve $AlPO_4$-11 in Real Time

Sandamini H. Alahakoon, Mathew J. Willans, and Yining Huang*

Cite This: *JACS Au* 2023, 3, 1670−1683

Read Online

ACCESS | Metrics & More | Article Recommendations | Supporting Information

ABSTRACT: Molecular sieves are crystalline three-dimensional frameworks with well-defined channels and cavities. They have been widely used in industry for many applications such as gas separation/purification, ion exchange, and catalysis. Obviously, understanding the formation mechanisms is fundamentally important. High-resolution solid-state NMR spectroscopy is a powerful method for the study of molecular sieves. However, due to technical challenges, the vast majority of the high-resolution solid-state NMR studies on molecular sieve crystallization are ex situ. In the present work, using a new commercially available NMR rotor that can withhold high pressure and high temperature, we examined the formation of molecular sieve $AlPO_4$-11 under dry gel conversion conditions by in situ multinuclear (^1H, ^{27}Al, ^{31}P, and ^{13}C) magic-angle spinning (MAS) solid-state NMR. In situ high-resolution NMR spectra obtained as a function of heating time provide much insights underlying the crystallization mechanism of $AlPO_4$-11. Specifically, in situ ^{27}Al and ^{31}P MAS NMR along with $^1H \rightarrow {}^{31}P$ cross-polarization (CP) MAS NMR were used to monitor the evolution of the local environments of framework Al and P, in situ $^1H \rightarrow {}^{13}C$ CP MAS NMR to follow the behavior of the organic structure directing agent, and in situ ^1H MAS NMR to unveil the effect of water content on crystallization kinetics. The in situ MAS NMR results lead to a better understanding of the formation of $AlPO_4$-11.

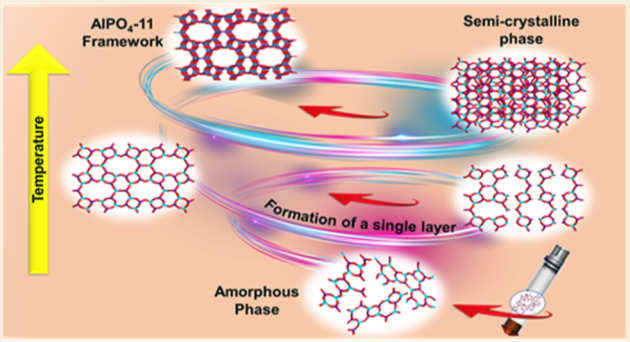

KEYWORDS: *molecular sieves, $AlPO_4$-11, in situ multinuclear NMR spectroscopy, crystallization*

INTRODUCTION

Molecular sieves such as zeolites and zeotype materials have periodic three-dimensional (3D) frameworks and well-defined pore structures. They have attracted much attention over the last several decades due to their versatile and intensive industrial applications in catalysis, ion exchange, gas storage, and chemical separations.[1−3] Typically, zeolites are referred to as a class of crystalline aluminosilicates constructed from silicate and aluminate tetrahedra.[4] In 1982, Wilson et al. discovered a type of zeolite-like molecular sieves, namely, aluminophosphates[5] as the first family of framework oxide molecular sieves without silica. Aluminophosphates ($AlPO_4$s) are highly crystalline microporous materials with pore diameters less than 2 nm. $AlPO_4$-based materials have an overall neutral framework due to their alternating AlO_2^- and PO_2^+ units.[6,7] One of the features of aluminophosphates is their ability to incorporate Si and other elements into the framework, creating a range of catalytically active sites.[8−10]

Molecular sieves are normally prepared under hydrothermal synthesis (HTS) conditions.[11−15] A better understanding of their formation mechanisms at a molecular level is crucial to designing new and engineering existing materials for targeted industrial applications. However, the formation mechanisms of zeolites and $AlPO_4$-based materials have long presented a challenge to researchers, owing to the fact that many chemical and physical processes occur in a heterogeneous medium involving gas, solution, and solid phases simultaneously.[16] Microporous materials including $AlPO_4$s are generally synthesized by transforming a hydrogel into a crystalline molecular sieve under HTS conditions. The extremely complex nature of crystallization involving numerous interrelated chemical reactions, equilibria, crystal nucleation, and growth processes in a heterogeneous medium within a closed reaction vessel limits one's ability to investigate the crystallization of molecular sieves under the HTS conditions.[16,17] This is particularly true for in situ studies as HTS is carried out in an autoclave, which makes directly monitoring the crystallization at elevated temperature and pressure difficult.

Over the years, several approaches have been developed to simplify the reaction systems, and examples include solvent-free synthesis and dry gel conversion (DGC).[18−28] In DGC,

Received: March 5, 2023
Revised: April 16, 2023
Accepted: April 21, 2023
Published: May 9, 2023

ACS Publications

© 2023 The Authors. Published by American Chemical Society

https://doi.org/10.1021/jacsau.3c00109
JACS Au 2023, 3, 1670−1683

Scheme 1. (a) Framework of $AlPO_4$-11, (b) *ab* Plane Viewed along the *c*-Axis, and (c) Projection of $AlPO_4$-11 Structure along the *c*-Direction with Three Crystallographically Non-Equivalent P Sites Shown

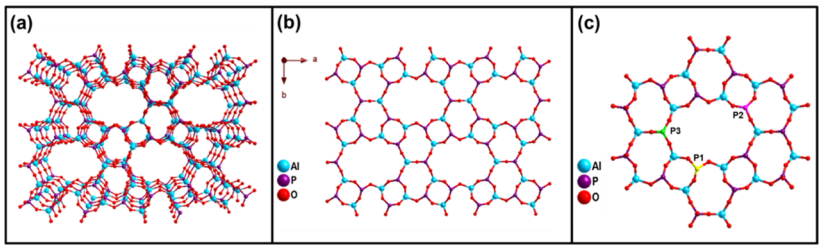

the starting dry gel often contains amorphous and/or semi-crystalline materials with desired framework elements and structure directing agent (SDA) that is physically separated from a small amount of water in an autoclave. The formation pathways of molecular sieves under DGC conditions are believed to be fundamentally similar to those under the HTS conditions as the dry gel powder usually contains 20−40% water by weight.[4,11,27,29] Many studies have shown that DGC is a good alternative method for evaluating crystallization as all the reactive species are now confined in the apparent solid phases, therefore simplifying the reaction systems. A small amount of water is physically separated from the dry gel, preventing the situation where the reactive species in the solution are in direct contact with solid gel from occurring. Furthermore, the small quantity of water from vapor and occluded in the gel is not enough to dissolve solids. Thus, the crystallization under DGC conditions is likely not due to gel dissolution. The lack of bulk water can effectively slow down the reactions by preventing a liquid phase and therefore limiting mass transport, facilitating the capture of intermediates.[30,31]

Due to the experimental challenges mentioned earlier, the vast majority of the studies reported in the literature were carried out by ex situ methods. One challenge is the identification and subsequent characterization of the true intermediates. Normally, in an ex situ study, the intermediates or precursors to the final crystalline microporous materials are captured by stopping crystallization followed by isolation of solids from the liquid phase. However, rapid quenching reactions may alter reactions and equilibria, leading to the species that may not have been otherwise relevant to the crystallization. On the other hand, some work in the literature reported that certain species that were observed by in situ measurements could not be seen in the quenched solids.[32−34] Furthermore, intermediates/precursors often involve cooperative weak interactions, and the post-synthetic treatments such as washing can alter their true structures, presenting uncertainty on if the solid species examined are the true intermediates. In recent years, many in situ approaches have been developed to provide unambiguous information on crystallization mechanisms. Various in situ techniques used for the study of molecular sieve crystallization include in situ time-resolved synchrotron X-ray powder diffraction,[35,36] in situ energy and angle-dispersive X-ray diffraction,[37,38] small- and wide-angle X-ray scattering,[39,40] in situ Raman[41,42] and in situ infrared spectroscopy,[43] in situ transmission electron microscopy,[44,45] and in situ atomic force microscopy.[32,46]

Solid-state NMR spectroscopy is a powerful technique for the characterization of molecular sieves.[47] It provides nuclide-specific information that is complementary to that obtained from X-ray diffraction-based methods as it probes short-range ordering in both crystalline and amorphous materials. Therefore, NMR spectroscopy is particularly suitable for investigating the formation of molecular sieves. However, compared with ex situ work, in situ NMR studies of molecular sieve crystallization have been rare due to many technical challenges such as leaking the fluid phase inside the NMR sample container, lack of mechanical resistance against pressure and temperature, harsh chemical environments, and high rotational speed instability. Despite these problems, much efforts have been made on developing in situ NMR methods for crystallization.[48−54] Several in situ studies (especially the early ones) were conducted using NMR cells that could only withstand moderate temperatures and pressures and operated only under static conditions.[55−61] To directly monitor the evolution of solid phases during crystallization in situ, various devices/rotors have been designed and utilized for conducting in situ crystallization under magic-angle spinning (MAS) conditions.[62−66] Recently, several NMR rotors that can withstand high temperature and high pressure (HTHP) have been designed for standard MAS probes.[67−70] These rotors essentially act as small autoclaves in which crystallization can take place. The rotors can be spun under MAS conditions, allowing high-resolution NMR spectra of a particular nucleus of interest in gaseous, liquid, and solids to be acquired simultaneously in real time. Several zeolitic materials such as $AlPO_4$-5, VPI-5, $AlPO_4$-8, zeolites mordenite, beta, and zeolites with LTA and FAU topologies have been examined.[17,34,47,68−78]

In this work, we present our study of the formation of microporous $AlPO_4$-11 by in situ solid-state NMR spectroscopy under MAS conditions. $AlPO_4$-11 is a representative aluminophosphate-based molecular sieve first synthesized by Union Carbide.[5] It has a unique framework topology (AEL) which is different from the known topologies of aluminosilicate zeolites. This framework has a unidimensional channel system with a non-circular 10-membered ring (6.7 × 4.4 Å)[79] (Scheme 1a,b). This sieve has shown potential for applications in ammonia alkylation with octanol-1 in the gaseous phase,[80] absorption of xenon gas,[81] and Knoevenagel condensation as a polymer/$AlPO_4$-11 nanocomposite catalyst.[81] SAPO-11 (derived by Si-substitution in the $AlPO_4$-11 framework) is an acid catalyst for alkylation, disproportionation, and isomerization involving aromatic compounds.[82,83] The crystallization of $AlPO_4$-11 and related systems under HTS and DGC conditions has been examined extensively, and much information on formation pathways was reported in the literature.[84−90] However, since all the details about crystallization for this sieve were obtained exclusively from ex situ studies, ambiguities do exist. An in situ study should provide direct unambiguous experimental evidence that can stand up to scrutiny. To this end, we carried out the in situ ^{1}H, ^{31}P, and

https://doi.org/10.1021/jacsau.3c00109
JACS Au 2023, 3, 1670−1683

^{27}Al MAS as well as ^{1}H → ^{31}P and ^{1}H → ^{13}C cross-polarization (CP) MAS NMR study of crystallization of $AlPO_4$-11 using an HTHP rotor. We chose crystallization inside the rotor (the reaction vessel) under a slightly modified DGC rather than typical HTS conditions. Specifically, the samples used in the in situ NMR study were prepared by mixing the pre-made dry gel with a small quantity of water. The sample remains as a solid powder without an apparent liquid phase upon mixing. The reasons for choosing the dry gel powder as a precursor for the crystallization study are several. Previous in situ NMR studies showed that under normal HTS conditions, as the reaction systems contain both liquid and solid phases, the observed spectra have the signals from the species in both phases.[57,58,77] Consequently, in some cases, efforts must be made to distinguish them in order to correctly interpret the data.[58,77,91] Such a situation can be avoided by using a dry gel powder precursor mentioned above as the ^{27}Al and ^{31}P spectra only have resonances of solid materials. An additional advantage is that since the amount of water is limited, the proton MAS NMR can easily be used to monitor the role of water in crystallization due to the lack of dominant water signals from the liquid phase. Finally, we previously conducted several detailed ex situ NMR studies on the formation of $AlPO_4$-11 under the DGC conditions which are very similar to this work.[86,88,92] The detailed information obtained from early work will be verified by this in situ study. A combination of the results from the previous ex situ and current in situ studies provides a better picture of the formation of this representative $AlPO_4$-based molecular sieves.

EXPERIMENTAL SECTION

Synthesis of Initial Dry Gel

$AlPO_4$-11 was synthesized using $Al(OH)_3$ (50% Al_2O_3, Sigma-Aldrich) and H_3PO_4 (85%, Sigma-Aldrich) as the Al and P sources. Di-*n*-propylamine (DPA, 99%, Alfa-Aesar) was used as SDA. The initial gel molar composition (Al_2O_3:P_2O_5:DPA:H_2O) was set to 1:1:1:40. A typical procedure[86] for the preparation of dry gel powder is as follows. An appropriate amount of $Al(OH)_3$ was mixed with distilled water, and the mixture was stirred at room temperature for 1 h, followed by dropwise addition of 85% H_3PO_4 and stirring for 1 h. Afterward, DPA was added dropwise with continuous stirring for 2 h. This mixture was then dried at 80 °C in an oil bath with constant stirring to allow evaporation of water until a white solid is formed. The solid sample was then ground into a fine powder, which will be, hereafter, referred to as the initial dry gel.

Crystallization of $AlPO_4$-11

Ex Situ Crystallization (in a Laboratory-Scale Autoclave). A series of samples were prepared by typically placing 1.0 g of the initial dry gel powder into a series of small Teflon cups. Each cup was placed in a Teflon-lined steel autoclave (volume, 23 mL) with 0.4 mL of distilled water at the bottom. The autoclaves were heated at 200 °C in an oven and taken out at different time intervals.

Ex Situ Crystallization (in a Glass Tube). To optimize the modified DGC method for in situ NMR studies, the initial dry gel of 1.0 g was mixed properly with 0.4 mL of water and packed into a glass tube (outer diameter: 5 mm; length: 3 cm). The glass tube was sealed (and placed inside an autoclave for safety reason). Then, a series of glass tubes containing the dry gel samples were heated at 200 °C in an oven. They were taken out at different time intervals for powder X-ray diffraction (PXRD) characterization after the reactions were quenched.

In Situ Crystallization (in an HTHP NMR Rotor). Initial dry gel weighing 1.0 g was mixed properly with approximately 0.4 mL of distilled water. This wetted solid sample was then packed into a 5 mm HTHP rotor and sealed properly for in situ MAS NMR experiments.

Characterization

PXRD patterns were recorded on either a Rigaku diffractometer using Cu Kα radiation (λ = 1.5418 Å) or a different Rigaku diffractometer with Co Kα radiation (λ = 1.7902 Å). Thermogravimetric analysis (TGA) measurements were performed under a N_2 atmosphere on a Mettler Toledo TGA/DTA851e instrument. The as-made $AlPO_4$-11 sample was heated from 25 to 390 °C at a rate of 10 °C/min.

All the ^{27}Al, ^{1}H, ^{13}C, and ^{31}P, MAS NMR measurements were carried out on a Varian/Chemagnetics Infinity Plus 400 WB spectrometer equipped with three rf channels operating at a field strength of 9.4 T. Depending on the requirement of the experiment, two MAS (a Varian 5 mm HFXY and a Varian 3.2 mm HXY) probes were used with a spinning rate of 4.7, 10, and 20 kHz. The magic angle was set using the ^{79}Br resonance of KBr. Larmor frequencies of ^{27}Al, ^{1}H, ^{13}C, and ^{31}P were 104.2, 399.9, 100.4, and 161.7 MHz, respectively. A Varian variable temperature control unit was used to set the temperature from 20 to 200 °C. At each temperature, 20 min of elapsed time was used to ensure the thermal equilibrium before beginning NMR spectra acquisition. A commercially available 5 mm HTHP rotor (Revolution NMR LLC) was used for in situ NMR experiments. It can be spun at a maximum spinning rate of 5 kHz and can withstand a temperature up to 240 °C and pressure up to 300 bar.

The chemical shifts were referenced externally to 1 M $Al(NO_3)_3$ solution (δ_{iso} = 0.00 ppm) and liquid ethanol as secondary standards using the peak of CH_3 at δ_{iso} = +1.11 ppm for ^{27}Al and ^{1}H, respectively. ^{31}P and ^{13}C chemical shifts were referenced to 85% H_3PO_4 (δ_{iso} = 0.00 ppm) and TMS (δ_{iso} = 0.00 ppm) using secondary standards of ammonium dihydrogen phosphate (δ_{iso} = +0.81 ppm) and adamantane (high-frequency peak, δ_{iso} = +38.60 ppm). The rf-field strength for ^{1}H decoupling was about 20 kHz for both ^{13}C and ^{31}P.

All the in situ NMR experiments were carried out in the Varian 5 mm HFXY probe with a spinning rate of 4.7 kHz. The ^{27}Al MAS spectra were acquired using a 45° of selective pulse length (0.7 μs), and 1600 scans were accumulated for each spectrum with a recycle delay of 0.25 s. ^{1}H MAS NMR spectra were recorded using a 90° pulse length of 7 μs, and four scans were accumulated for each spectrum with a 5 s recycle delay. ^{1}H → ^{13}C CP MAS NMR spectra were recorded with a contact time of 2.5 ms, and 180 scans were accumulated with a recycle delay of 10 s. The ^{1}H 90° pulse length of 10 μs and the Hartmann−Hahn condition[93] were determined using adamantane. ^{31}P MAS NMR spectra were recorded using a short excitation pulse of 30° with two-pulse phase modulation (TPPM) decoupling, and 32 scans were accumulated with a 30 s recycle delay. The rf field strength for ^{1}H decoupling was about 20 kHz. The ^{1}H → ^{31}P CP MAS NMR spectra were recorded with a contact time of 15 ms, and 64 scans were accumulated with a recycle delay of 10 s. The ^{1}H 90° pulse length of 7 μs and the Hartmann−Hahn condition were determined using $(NH_4)H_2PO_4$.

The ex situ ^{27}Al and ^{31}P MAS NMR measurements were carried out using the same 5 mm HFXY MAS probe. For ^{31}P MAS experiments, a 30° pulse was typically used, and the recycle delay was 60 s. The ^{27}Al MAS spectra were acquired using a 45° of selective pulse and a pulse delay of 1 s. The 5 mm HFXY MAS probe was used to obtain the ^{1}H MAS NMR spectra with the spinning rates of 4.7 and 10 kHz while a 3.2 mm HXY MAS probe employed for reaching a spinning rate of 20 kHz. Typically, the ^{1}H MAS NMR spectra were recorded using a 90° excitation pulse with 10 s of recycle delay.

RESULTS AND DISCUSSION

As mentioned earlier, the present in situ multinuclear MAS NMR study was carried out using a dry gel as a reaction precursor for crystallization, in order to simplify the reaction system and avoid large apparent liquid phase. The dry gel used was prepared according to the procedure described in the literature.[86] Before in situ MAS NMR experiments, the crystallization at 200 °C under ex situ conditions was performed to ensure that the dry gel prepared could be

https://doi.org/10.1021/jacsau.3c00109
JACS Au 2023, 3, 1670−1683

transformed into $AlPO_4$-11 as expected. The PXRD patterns of the solid materials captured ex situ as a function of crystallization at 200 °C are shown in Figure S1, and they are consistent with those reported before.[86,88] The selected ^{31}P and ^{27}Al MAS spectra of the dry gel samples heated for different times are shown in Figure S2. The dry gel samples have the same NMR spectroscopic signatures as reported.[86] The ex situ results clearly indicate that the dry gel prepared can indeed be converted to $AlPO_4$-11 in about 6 h at 200 °C, a time period that is highly suitable for in situ study.

In the standard DGC method mentioned above, the crystallization is carried out in an autoclave where the dry gel is physically separated from a small amount of water (Scheme S1). When doing it inside an NMR rotor, water can no longer be separated from the dry gel. Therefore, the required amount of water was directly mixed with the dry gel. After dispersing the water thoroughly within the dry gel, the dry gel powder was packed into the NMR rotor. To mimic the reaction environment inside an NMR rotor, ex situ crystallization was carried out by packing the dry gel in several glass tubes with dimensions similar to the 5 mm NMR rotor (outer diameter: 5 mm; length: 3 cm). The tubes were then sealed and heated at 200 °C for different times. The PXRD patterns of the quenched samples indicate that the reflections due to $AlPO_4$-11 started appearing after 2 h of heating, and the crystallization nearly completed after 6 h (Figure 1).

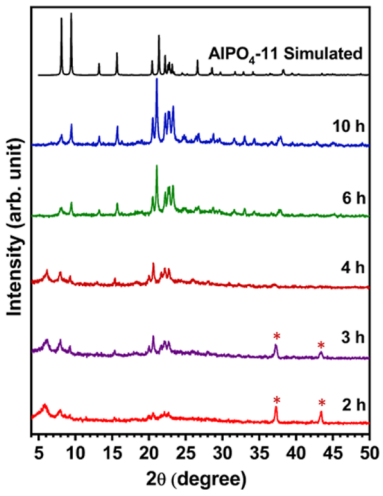

Figure 1. Powder XRD patterns of selected dry gel samples crystallized at 200 °C inside sealed-glass tubes. The PXRD patterns were obtained using Cu Kα radiation (λ = 1.5418 Å). (*) Asterisks denote the signals from the sample holder.

After modifying and optimizing the DGC conditions for in situ study, the crystallization was carried out inside the NMR rotor under MAS conditions. The system was heated from 20 to 200 °C. Once the desired temperature, i.e., 200 °C was reached, the crystallization was allowed for 15 h. Figure 2a illustrates the in situ ^{27}Al MAS spectra of the dry gel heated at different temperatures and durations. The ^{27}Al MAS spectrum of the initial dry gel at 20 °C, as shown in Figure 2a, consists of three rather broad signals at −10, 9, and 45 ppm. The overall spectral appearance looks similar to those of dry gel prepared under similar conditions in this work (Figure S2) and reported in the literature.[86] The −10 and 45 ppm peaks are due to the octahedral $Al(OP)_4(H_2O)_2$ and tetrahedral $Al(OP)_4$ in solid aluminophosphate species, respectively.[77,86,94,95] The peak at 9 ppm is assigned to unreacted alumina.[92] Upon heating from 20 to 140 °C, the tetrahedral Al peak increases its intensity at the expense of octahedral Al, indicating that as soon as heating starts, the octahedral Al is quickly converted to tetrahedral Al via dehydration. It should be pointed out that the in situ NMR study allows one not only to observe what is happening at crystallization temperature (i.e., 200 °C) but also to monitor the reactions at temperatures below 200 °C. The information from temperatures lower than crystallizing temperature usually is not easily available from ex situ studies.

Treating the initial dry gel for 30 min at 200 °C yields a new peak at 36 ppm which is characteristic of tetrahedral Al in $AlPO_4$-11. Its intensity gradually increased with increasing heating time, indicating that more gel is converted to $AlPO_4$-11 with increasing crystallization time. In the current in situ study, the 36 ppm peak belonging to $AlPO_4$-11 appeared in the spectrum after 30 min heating, whereas in the ex situ study, the reflections characteristic of $AlPO_4$-11 in PXRD patterns can only be observed after 2 h heating at 200 °C (Figure S2). Accompanying the 36 ppm peak, another new sharp peak at 49 ppm appeared at 200 °C. This new peak can be attributed to a five-coordinated aluminum complex bonded to HPO_4^{2-} ions in solution.[55,77,96] This assignment is consistent with the concomitant observation of a small sharp ^{31}P signal at −2.4 ppm at 200 °C in the in situ ^{31}P MAS spectra (Figure 2b), which is due to the P in the abovementioned species.[96] As mentioned earlier, the dry gel does contain occluded and added water. Therefore, heating at 200 °C may result in small localized pools of water containing the AlPO species within the gel. Heating the gel at 200 °C under autogenous conditions leads to the reorganization of the gel structure via bond breaking and reforming, yielding the observed species. The fact that the intensities of both 49 ppm Al signal and −2.4 ppm P resonance in their respective in situ MAS spectra do not vary significantly with increasing heating time implies that the small liquid domains are saturated with the AlPO species formed during the crystallization at 200 °C and are in reaction equilibrium with solids. The ^{27}Al sharp peak at 49 ppm was also observed during the formation of $AlPO_4$-5[77] and SAPO-34,[57] and it was interpreted as an AlPO species acting as a nutrient that is in equilibrium with the nucleates of targeted molecular sieves. Another new feature in the in situ ^{27}Al MAS spectra at 200 °C is a broad peak near 12 ppm whose intensity increases with increasing heating time. This signal can be attributed to the penta-coordinated Al in solids with $Al(OP)_4(H_2O)$ environment.[84,90] The broadness of the peak suggests a distribution of local geometry around five-coordinated Al. In situ ^{27}Al MAS spectra clearly indicate that $AlPO_4$-11 forms after 30 min of crystallization at 200 °C.

In situ ^{31}P MAS NMR is used to monitor the evolution of P local environment in the dry gel as a function of heating temperature and time, and the spectra are shown in (Figure 2b). The ^{31}P MAS spectrum of dry gel before heating possesses several signals: a sharp narrow resonance at −2 ppm overlapping with a broad resonance centered at around −12 ppm with a broad shoulder at around −18 ppm. The broad signal at −12 ppm and its −18 ppm shoulder represent P atoms in the amorphous and semi-crystalline AlPO phases with a lower degree of condensation, i.e., $P(OAl)_x(OH)_{4-x}$ (where x = 2−3). The broadness of these signals reflects that the P atoms have large bond angle and length distributions, which is consistent with the amorphous nature of the sample. Previous comprehensive ex situ SSNMR studies of $AlPO_4$-based

https://doi.org/10.1021/jacsau.3c00109
JACS Au 2023, 3, 1670−1683

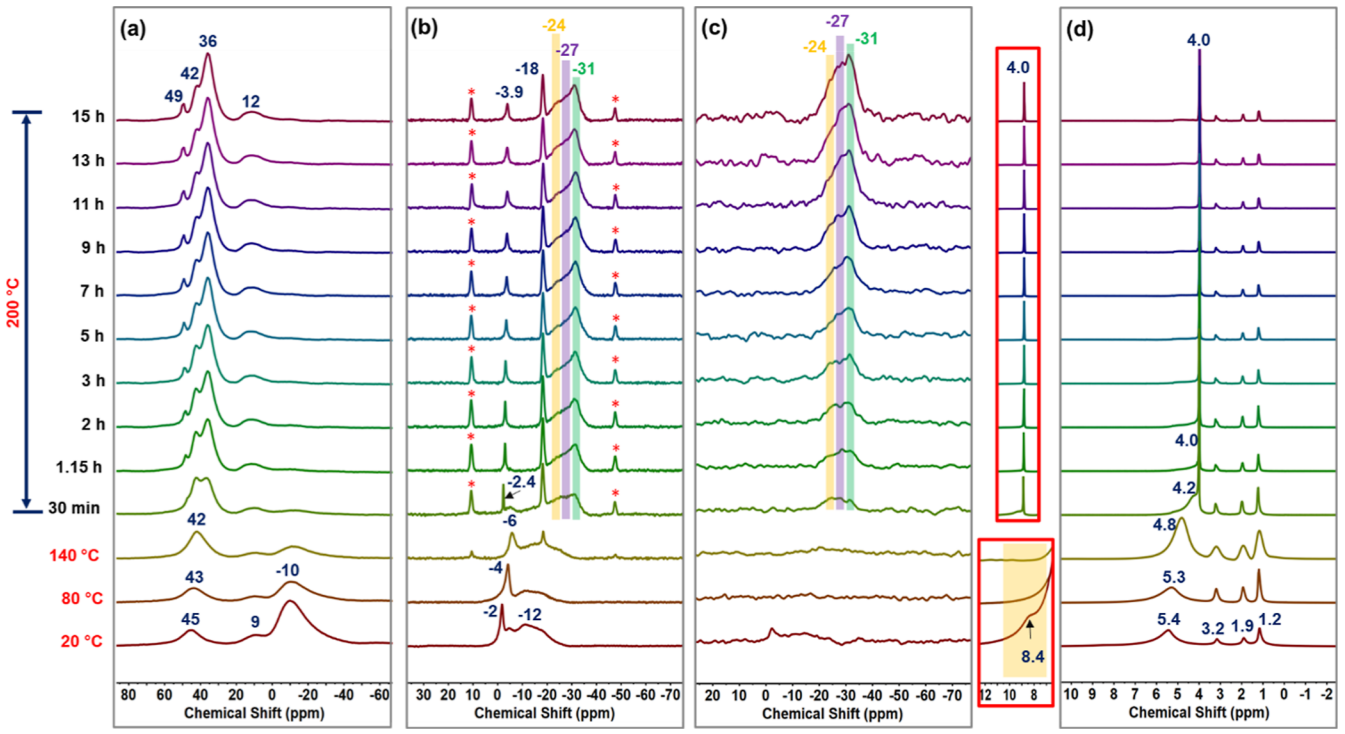

Figure 2. In situ NMR spectra of dry gel samples (1.0 g) mixed with additional 0.4 mL of water: (a) ^{27}Al MAS, (b) ^{31}P MAS, (c) ^{1}H → ^{31}P CP MAS, and (d) ^{1}H MAS spectra. The spinning rate is 4.7 kHz. (*) Asterisks denote the spinning sidebands. Top inset: intensity scaled liquid water peak (4.0 ppm) in ^{1}H MAS NMR spectra. Bottom inset: vertically enlarged ^{1}H MAS NMR spectra at 20, 80, and 140 °C showing the peak corresponding to protonated DPA (8.4 ppm).

molecular sieves (including $AlPO_4$-11 and $AlPO_4$-5) showed that under similar DGC conditions, the ^{31}P MAS spectrum of the initial dry gel also contains a broad resonance spanning from approximately 0 to −25 ppm with a maximum of the profile at about −12 ppm. Through thorough characterization using advanced 2D NMR and computational methods, several individual resonances were identified as part of the broad profile, and they were assigned to the P sites in the linear tetrahedral Al and P units $[(P{-}O{-}Al)_n]$ in the gel and those in the four- and six-membered ring that are in the 1D chains.[22,86,90]

The sharp −2 ppm peak is worth commenting on. Since the corresponding proton spectrum (Figure 2d) clearly shows that there is no liquid water phase in the initial gel before heating, this sharp peak must be part of the solids. This peak is likely due to the phosphate group (e.g., $H_2PO_4^-$ or HPO_4^{2-}) attached to a single Al in the solids, and the sharpness of this peak reflects its high mobility.[96] Upon heating from 20 to 140 °C, the −2 ppm peak becomes slightly broader and shifts to the lower chemical shift to −6 ppm. It seems that the phosphate species interact with more Al sites and become less mobile with heating at higher temperatures. Meanwhile, between 20 and 140 °C, the center of the broad envelope gradually shifts to a lower chemical shift, suggesting that the degree of condensation at P increases. A sharp signal at −18 ppm starts to emerge at 140 °C. Heating the dry gel at 200 °C for 30 min results in a drastic change in the ^{31}P MAS spectrum. It comprises a peak at −31 ppm with a broad shoulder at −27 ppm. The −18 ppm peak becomes very sharp and strong. There is also a sharp new peak at −2.4 ppm. The −18 ppm peak has been identified as a P site in a layered intermediate in $AlPO_4$-11 synthesis under DGC conditions.[22,86] In addition to $AlPO_4$-11, it is also captured during the synthesis of many other sieves under ex situ conditions including $AlPO_4$-5, $AlPO_4$-18, SAPO-5, SAPO-11, SAPO-34, SAPO-37, etc.[22,26,97−102] The nature of this −18 ppm resonance captured in many in situ and ex situ NMR studies of the formation of $AlPO_4$-based sieves has been thoroughly characterized and was identified as the P site with the $P(OAl)_3(OH)$ coordination environment in a semi-crystalline layered phase. In the present in situ study, since small liquid water domain(s) may exist, as suggested by the corresponding ^{1}H NMR spectrum (Figure 2d), the question is whether the very sharp −18 ppm is in the liquid or solid phase. An inspection of the ^{31}P MAS spectrum reveals that this peak has two strong spinning sidebands (SSBs), which clearly indicates that this P is in solids. On the other hand, the −2.4 ppm peak is also very sharp but exhibits no SSBs. Thus, we assign this signal at −2.4 ppm to a P species in a small liquid water pool localized in the gel, preassembly $Al(H_2O)_5(H_3PO_4)$ and $Al(H_2O)_5(HPO_4)$ or more likely the average of the two.[57,96] The Al in these species corresponds to the 49 ppm peak in the corresponding ^{27}Al MAS spectrum. Careful inspection of the in situ ^{31}P MAS spectra reveals that the position of this peak gradually shifted to lower chemical shift direction over time from −2.38 to −3.96 ppm within 15 h at 200 °C (Figure S3). This small change in the chemical shift is likely due to the slight change in pH of the small liquid water pool as the crystallization proceeds. The appearance of the peak at −31 ppm together with the shoulder at −27 ppm is characteristic of crystalline $AlPO_4$-11. Seeing these signals clearly indicates the formation of the AEL structure after 30 min of heating at 200 °C. Further increase in crystallization time does not lead to significant changes in the spectrum except that the intensity of the peak due to $AlPO_4$-11 increases with an increase in heating time. It is worth noting that although the Al and P resonances that are characteristic of

https://doi.org/10.1021/jacsau.3c00109
JACS Au 2023, 3, 1670−1683

$AlPO_4$-11 were observed in their respective ^{27}Al (36 ppm) and ^{31}P (−31 ppm) MAS spectra of the samples heated for 30 min, 1.15 h, and 2 h, the corresponding PXRD patterns obtained in ex situ study did not show any reflections due to $AlPO_4$-11. It appears that although long-range ordering associated with the AEL structure can only be detected by XRD after heating the dry gel at 200 °C for 3 h or longer, the local structures of Al and P atoms in the gel heated for less than 3 h have already evolved to be very close to those in the AEL structure. The sample spinning may also have the same effect as agitation/tumbling, leading to a faster crystallization. It is also worth noting that the intensity of the very broad signal centered at around −12 ppm in the initial dry gel decreases upon heating, and the intensity of the new sharp peak that appeared at −18 ppm at 140 °C increases with heating at the expense of the broad −12 ppm signal. This observation indicates that the 1D chains with four- and six-membered rings in the dry gel were gradually consumed or, in the other words, the 1D chains were gradually cross-linked together to form the 2D layered intermediate that eventually transforms into the 3D AEL structure. A similar pathway has been proposed in the literature based on the ex situ results.[86,90,92] The present in situ results are unambiguously consistent with those of previous work.

To further characterize various P species, an in situ $^1H \rightarrow {}^{31}P$ CP MAS experiment was also carried out. In addition to sensitivity enhancement, CP is also a technique for spectral editing. Our previous work has shown that compared to the as-made $AlPO_4$-11, the amorphous and semi-crystalline AlPO materials have a much shorter proton spin−lattice relaxation time in the rotating frame ($T_{1\rho}{}^H$).[86,92] Therefore, $^1H \rightarrow {}^{31}P$ CP experiment with a long contact time should discriminate against the phases with short $T_{1\rho}{}^H$. The CP spectra acquired with a long contact time of 15 ms (Figure 2c) look drastically different from the one-pulse MAS spectra. Specifically, two sharp peaks at −2.4 and −18 ppm along with associated SSBs vanish in the CP spectra. This is because the signal at −18 ppm belonging to the semi-crystalline phase is known to have a very short $T_{1\rho}{}^H$, resulting in the fast decay of the CP signal at longer contact times.[86] −2.4 ppm resonance originates from the species in small liquid domains, and the tumbling in liquid averages out the $^1H-{}^{31}P$ dipolar interaction. The very broad resonances observed in the one-pulse MAS spectra of the samples heated at temperatures below 200 °C do not appear in the corresponding CP spectra because they belong to amorphous materials that also have a short $T_{1\rho}{}^H$.[86,92]

The CP spectrum of the dry gel heated for 15 h at 200 °C looks identical to that of the crystalline $AlPO_4$-11 reported in the literature.[86,88,90,92,103] $AlPO_4$-11 crystallizes in an orthorhombic crystal system with a space group of *Imma*. Its unit cell has three crystallographically inequivalent P sites (Scheme 1c) with an occupancy of P3:P2:P1 = 1:2:2. The P3 site is in the junction of two adjacent six-membered rings. Both P1 and P2 are in the junction of the six- and four-membered rings with the same site occupancy. In the ^{31}P MAS spectrum of $AlPO_4$-11, these three sites manifest themselves as an asymmetric broad peak with a maximum at −31 ppm and a weaker shoulder at around −27 ppm. In the literature, this broad asymmetric envelope can be deconvoluted into three peaks at −24, −27, and −31 ppm, which are assigned to P3, P2, and P1, respectively.[88]

The CP spectra indicate that no $AlPO_4$-11 is formed when the dry gel is heated between 80 and 140 °C. The signal corresponding to $AlPO_4$-11 only appears in the CP spectrum when the temperature reaches 200 °C. The intensity of the peak belonging to $AlPO_4$-11 increases with increasing heating time at 200 °C, implying that the dry gel is continuously converted to $AlPO_4$-11 with increasing crystallization time. It is worth noting that for the CP spectra of the samples heated at 200 °C for 3 h and longer, all three P sites are visible, consistent with the formation of $AlPO_4$-11 which is also indicated by the ex situ PXRD patterns of the samples prepared under the same conditions.

However, the CP spectra of the dry gel heated for 30 min, 1.15 h, and 2 h look different from those of simple MAS spectra in the region where the signals due to $AlPO_4$-11 appear. Specifically, the peaks at −24 and −27 ppm corresponding to P3 and P2 sites have stronger intensity compared with the resonance at −31 ppm due to the P3 site. This result suggests that when $AlPO_4$-11 begins to crystallize, the framework formed in the early stage is not homogeneous. The portion containing P3 and P2 sites has fully condensed P with the $P(OAl)_4$ environment, i.e., each P is bound to four Al atoms via bridging oxygens. The region(s) mainly contains P3 and P2 appear to be better developed with their local environments closer to the fully crystallized product. Therefore, the $T_{1\rho}{}^H$ values of these two sites are relatively long, making them visible in both the MAS and CP spectra. P1 site, on the other hand, likely has a much shorter $T_{1\rho}{}^H$ because it is located in an area where its local structure is very similar to but not yet in the state of completely crystalline $AlPO_4$-11.

Previous work suggested that the 3D AEL framework is formed from the stacking of the 2D sheets very similar to the *ab* plane of $AlPO_4$-11.[86] The sheets (or layers) form first. Cross-linking between the layers, however, takes place later, and the initial 3D structure along the channel direction is disordered. The CP behavior of P1 sites seems to suggest that the formation of proper Al−O−P linkages along the channel direction involving P1 is the last step. Thus, in the early stage of the crystallization, P1 does not form four strong P−O−Al covalent bonds, which results in a shorter $T_{1\rho}{}^H$ in the early crystallization, leading to a weak CP signal when a long contact time is used. The reason this P site is the final step for the cross-linking is that this particular P at the junction of the four- and six-membered rings is shielded by the SDA molecule.[88]

In situ ^1H MAS NMR spectra are shown in Figure 2d. At 20 °C, there are five peaks in the spectrum. The signals at 1.2, 1.8, and 3.2 ppm originate from the SDA molecule occluded in the solids (Scheme S2). The peaks at 1.2 and 1.8 ppm can be assigned to the protons on the methyl groups and the methylene fragment next to the CH_3 group. The resonance at 3.2 ppm is due to the protons in the methylene group directly bound to the nitrogen atom in the NH_2^+ group.[90] The broad signal centered around 5.4 ppm in the initial gel is a combination of resonances from adsorbed water, coordinated water, and the exchanged signals between water, POH, and AlOH.[77] The broad shoulder peak at 8.4 ppm is assigned to the protons on the NH_2^+ group of protonated amine ($DPAH^+$).[89,104] Heating at 80 and 140 °C does not seem to significantly affect the three peaks at 1.2, 1.8, and 3.2 ppm given by the SDA. However, as soon as heating begins at 80 °C, the 8.4 ppm signal disappeared immediately, suggesting that the protonated amine is converted to a neutral amine form via deprotonation. Through a thorough ex situ NMR study, Deng et al. proposed that the SDA (DPA) initially exists in its protonated form ($DPAH^+$) in the layered phase. This 2D

https://doi.org/10.1021/jacsau.3c00109
JACS Au 2023, 3, 1670−1683

material subsequently transforms to $AlPO_4$-11 where $DPAH^+$ is deprotonated, and two DPA molecules form a dimer in the 10-ring channels of the framework.[90] Our in situ work indicates that deprotonation indeed occurs in solids upon heating, but it happens before the layered phase forms under the conditions used in this study. It appears that deprotonation is part of the process where the 1D chains join together to form the layered material. Another change is that the broad signal at 5.4 ppm observed at 20 °C shifted to 4.8 ppm at 140 °C. As mentioned earlier, this broad resonance results from a number of species, such as occluded water, P−OH, Al−OH, $Al-OH_2$, etc., among which they interact with each other via hydrogen bonding. The observed shift in the peak position toward lower chemical shift with increasing temperature suggests an increased rate of the proton exchange among these species and weakened hydrogen bonding, indicating that the structure of the gel undergoes reorganization.

It is worth noting that no liquid water signal was observed in the ^1H MAS NMR spectra of the dry gel in the temperature range between 20 and 140 °C, indicating no apparent liquid water phase existing up to 140 °C. This result indicates that the small amount of water mixing with the dry gel before heating appears to be highly dispersed in the dry gel powder, and this added water interacts with the gel. To confirm this conclusion and better understand the ^1H MAS NMR spectra, ex situ ^1H NMR (both static and MAS) experiments were carried out on dry gel with and without additional 0.4 mL of water (Figure S4). The static spectrum of the dry gel without additional water shows an extremely broad peak, indicating that the water molecules are very rigid. TGA confirmed that the initial dry gel powder contains ca. ∼20% water by weight (Figure S5). This peak becomes narrower upon spinning the sample at 4.7, 10, and 20 kHz. The static proton spectrum of the dry gel (1.0 g) mixed with additional 0.4 mL of water without heat treatment contains two resonances at 5.7 and 1.0 ppm. The 1.0 ppm resonance is likely due to the methyl protons of the SDA. No liquid water signal was observed. These signals are much narrower than that in the dry gel without additional water, implying that the mobility of the proton-containing species in solids increases with the addition of water. The MAS spectra spun at 4.7, 10, and 20 kHz exhibit higher resolution, and the resolution increases with spinning speed. These results clearly suggest that when the additional 0.4 mL of water was added to the dry gel powder, water is uniformly dispersed within the dry gel, and no liquid water exists. However, adding additional water does mobilize all the proton-containing species (especially the SDA) in the solids.

When the crystallization begins at 200 °C, again major changes occurred in the in situ ^1H MAS spectra. The broad resonance now moved further toward the lower chemical shift direction from 5.4 to 4.2 ppm. This peak shift implies significant reorganization of various proton-containing species inside the dry gel. Concomitantly, a very sharp strong peak emerged at 4.0 ppm, which indicates the formation of a small amount of liquid water in the rotor[105] as the corresponding time domain signal has a component with a very long-lived free induction decay, typical of liquid water (Figure S6). Forming a small liquid phase of water is due to several reasons. The main reason is that breaking the hydrogen bonding between occluded/adsorbed water and the solid gel frees up water molecules at elevated pressure and temperature. Condensation of P−OH and Al−OH groups to form proper P−O−Al linkages in the framework yields additional water molecules. Furthermore, the conversion of the octahedral Al, $Al(OP)_4(OH_2)_2$, to tetrahedral Al, $Al(OP)_4$, also releases water molecules. The peak position of water formed inside the rotor (4.0 ppm) is slightly different from pure liquid water (4.7 ppm), which might be due to the pH resulting from crystallization as it is known that the ^1H chemical shift of liquid water shifts to lower chemical shift when pH increases.[105] It is noticed that the three peaks belonging to the DPA are very well resolved at a low spinning rate of 4.7 kHz, which suggests that the SDA molecules are rather mobile in the entire temperature range and heating periods. The peak at around 8.4 ppm due to the protons of the NH_2^+ group did not reappear, suggesting that the SDA stays as neutral amine and protonated amine did not reform, confirming that it is the neutral DPA that exists in both layered phase and final $AlPO_4$-11 framework.

After the in situ MAS NMR experiments were completed, the solid sample was recovered and characterized using powder XRD. The diffraction pattern observed is shown in Figure 3,

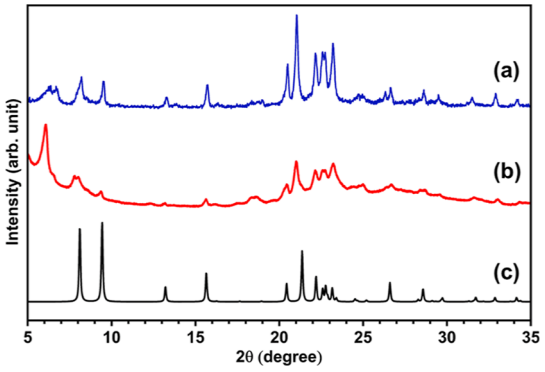

Figure 3. Powder XRD patterns of the samples recovered after the in situ crystallization: (a) with additional 0.4 mL of water; (b) with additional 0.1 mL of water; and (c) simulated $AlPO_4$-11. The PXRD patterns were obtained using Cu Kα radiation (λ = 1.5418 Å) except for that in (b) which was obtained with Co Kα radiation (λ = 1.7902 Å). The 2θ values were converted to those corresponding to Cu Kα radiation for comparison.

clearly indicating that the product is indeed $AlPO_4$-11 with good crystallinity. In addition to the reflections belonging to $AlPO_4$-11, there are two weak low angle peaks at around 6−7° belonging to the layered semi-crystalline intermediate phase reported in a previous DGC study of $AlPO_4$-11,[86] indicating that most of the layered material has transformed to $AlPO_4$-11.

To further evaluate the role of the water in the crystallization process, an additional in situ NMR experiment was carried out by adding less amount of additional water (0.1 mL) to the initial gel (1.0 g) and heating this sample for 2.15 h at 200 °C. When 0.1 mL of water was added to 1.0 g of dry gel, the in situ ^{27}Al, ^{31}P and ^1H spectra below 200 °C (i.e., 20, 80, and 140 °C) are very similar to those of dry gel with 0.4 mL of water heated for the same period of time (Figure 4). However, when the temperature reached 200 °C (the crystallization temperature), significant differences were observed. In the ^{27}Al spectra (Figure 4a), there is only a single broad peak at 39 ppm seen in the tetrahedral Al region. For the fully crystallized $AlPO_4$-11, its tetrahedral Al appears at 36 ppm rather than at 39 ppm. It seems that this broad peak at 39 ppm is due to the overlapping of the 42 and 36 ppm peaks observed for the sample with 0.4 mL of water. These results indicate that compared to the

https://doi.org/10.1021/jacsau.3c00109
JACS Au 2023, 3, 1670−1683

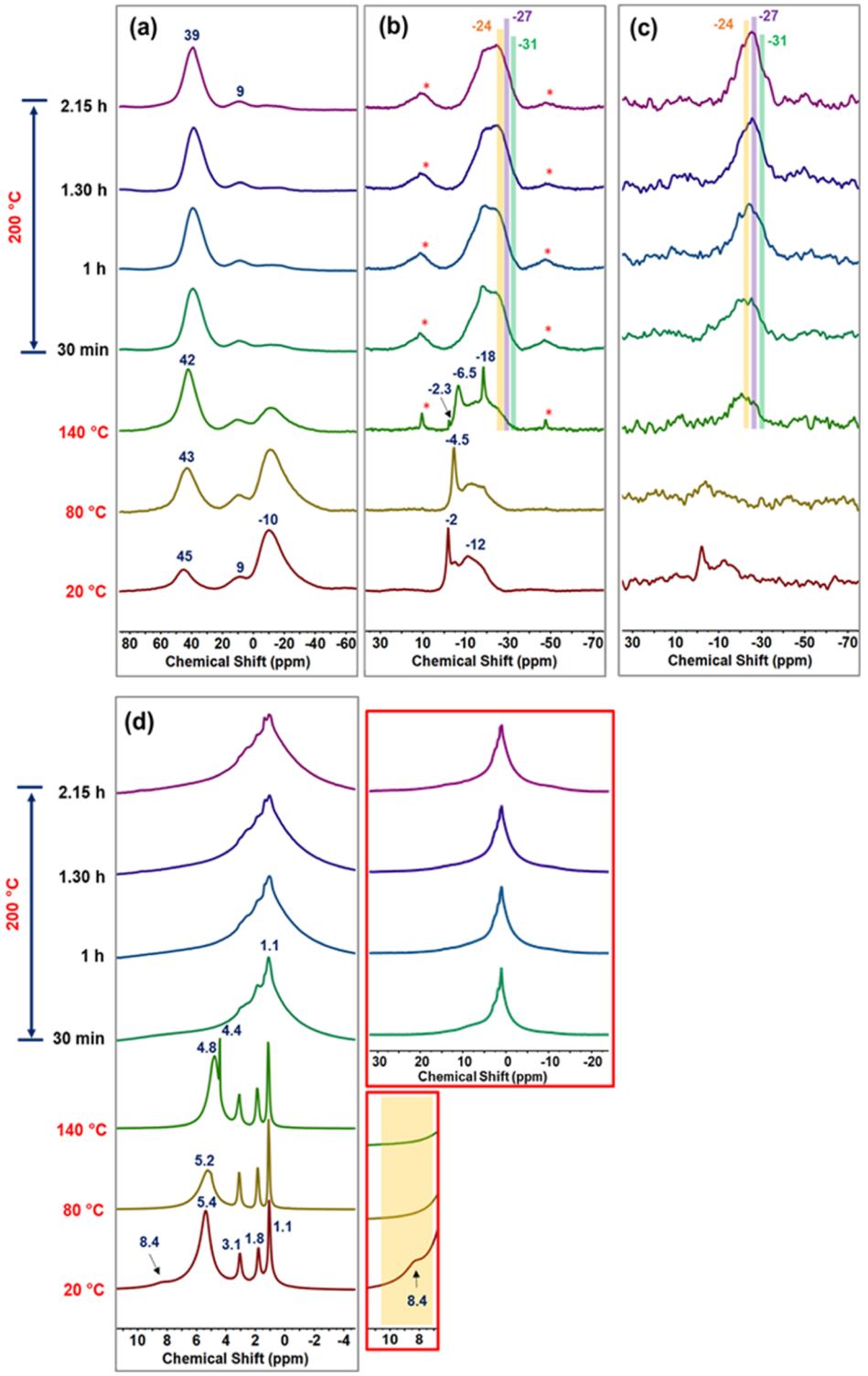

Figure 4. In situ NMR spectra of dry gel samples (1.0 g) mixed with additional 0.1 mL of water: (a) ^{27}Al MAS; (b) ^{31}P MAS; (c) ^{1}H → ^{31}P CPMAS; and (d) ^{1}H MAS NMR spectra. The spinning rate is 4.7 kHz. (*) Asterisks denote the spinning sidebands. Top inset: ^{1}H MAS NMR spectra acquired at 200 °C on a wider scale. Bottom inset: vertically enlarged ^{1}H MAS NMR spectra acquired at 20, 80, and 140 °C showing the peak corresponding to protonated DPA (8.4 ppm).

sample with 0.4 mL of additional water, the sample with less water contains a smaller amount of $AlPO_4$-11 upon heating for about 2 h.

^{1}H MAS spectra at 200 °C of the dry gel sample mixed with additional 0.1 mL of water (Figure 4d) have very broad peaks, suggesting that less water results in significantly reduced mobility of the proton-containing species including the SDA. The major difference between the samples containing 0.4 and 0.1 mL of water is the absence of the sharp peak at around 4 ppm, indicating the absence of a liquid water phase in the sample with 0.1 mL of water. This is likely due to (1) the amount of the water molecules bound to the gel surface via

https://doi.org/10.1021/jacsau.3c00109
JACS Au 2023, 3, 1670−1683

hydrogen bonding that can be released upon heating at high temperatures is much less. (2) The rates of various reactions become lower, resulting in less water produced.

The differences in the in situ ^{31}P MAS spectra are also interesting (Figure 4b). The spectra at 140 °C and below are almost identical to that of the sample containing 0.4 mL of water. However, at 200 °C, the sample with 0.1 mL of water exhibits a very broad profile with two overlapping signals at −18 and −24 ppm. The −24 ppm peak also has a shoulder at −31 ppm. This shoulder became more obvious with increasing heating time. The −18 ppm peak is due to the layered materials. What is interesting is that when there is more water available, the layered phase will become highly crystalline as the spectra of the sample with 0.4 mL of water exhibit a very sharp line at −18 ppm with intense SSBs. For the sample with 0.1 mL of water, the sharp −18 ppm peak only briefly appeared at 140 °C. It immediately becomes very broad as soon as the temperature reached 200 °C. The peak at −24 ppm and its shoulder at −31 ppm suggest the formation of $AlPO_4$-11. Indeed, the PXRD pattern of recovered samples shows that the sample heated at 200 °C for 2.15 h is a mixture of layered phase and $AlPO_4$-11 (Figure 3a). The reflections due to $AlPO_4$-11 are rather broad, indicating that the $AlPO_4$-11 just begins forming and has lower crystallinity and/or that the sizes of crystallites are fairly small. Since the −24 ppm peak coincides with the P3 site, the ^{31}P MAS spectra clearly indicate that this P site in $AlPO_4$-11 develops first, due to that with less amount of water the crystallization rate is slower. In situ ^{31}P MAS NMR allows us to capture the formation of $AlPO_4$-11 at a very early stage where only the P3 site is fully formed, but the P1 site just begins to develop. The ^{1}H → ^{31}P CP spectra further confirm the above interpretation. The peak at −18 disappears, but three sites due to $AlPO_4$-11 at −24, −27, and −31 ppm signals are clearly visible with the peak at −31 ppm having the smallest intensity. It seems that adding less water to the dry gel does not prevent $AlPO_4$-11 crystallization from occurring. However, the reaction rates apparently are reduced. This result obtained from in situ NMR is further supported by ex situ PXRD data. Figure S7 clearly shows that the formation of $AlPO_4$-11 from the dry gel samples with 0.1 mL of additional water per 1.0 g of dry gel is much slower than the dry gel with 0.4 mL of water (Figure 1).

We also wish to point out that the small amount of liquid water formed can only be observed in situ, i.e., at crystallization temperature (Figure 2d). This was confirmed by an ex situ experiment where the dry gel (1.0 g) with 0.4 mL of additional water added was allowed to crystallize at 200 °C for 1 day. ^{1}H MAS spectrum was obtained immediately upon cooling the sample to room temperature. As shown in Figure 5, the ^{1}H MAS spectrum of the ex situ sample (Figure 5a) looks similar to the in situ sample before heating (Figure 5b). The three peaks belonging to the SDA appear at the same positions in both samples. However, the broad peak at around 8.4 ppm that is present in the in situ sample before heating is absent in the ex situ sample. This result is consistent with the results discussed above, suggesting that the SDA exists in the form of neutral amine, rather than protonated DPA.

Furthermore, the sharp peak observed at 4.0 ppm in the in situ spectrum at 200 °C (Figure 5c) did not appear in the spectrum of the ex situ sample after heating, indicating the absence of a liquid water domain in the latter sample. There is a peak at 5.5 ppm corresponding to the water adsorbed in the gel. The position of the peak is very much different from the broad resonance at 4.2 ppm in the in situ spectrum at 200 °C for 15 h and closer to the 5.4 ppm peak of the initial dry gel. These results show that the liquid water only forms at 200 °C and can only be observed via in situ NMR experiments. When cooling the sample to room temperature, the water molecules are adsorbed again on the surface of the solids and therefore cannot be seen via ^{1}H MAS NMR.

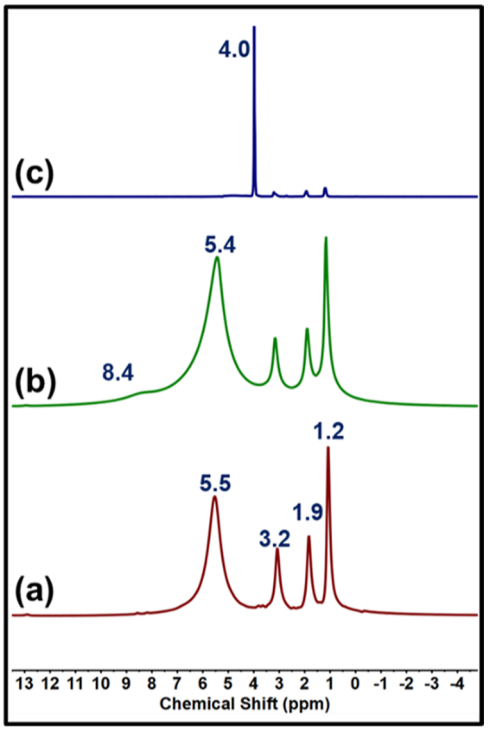

Figure 5. ^{1}H MAS NMR spectra of selected $AlPO_4$-11 gel samples: (a) ex situ: initial dry gel mixed with 0.4 mL of additional water and crystallized for 1 day at 200 °C. The spectrum was taken immediately after cooling to room temperature; (b) in situ: initial dry gel mixed with 0.4 mL of additional water. The spectrum was taken inside the rotor at 20 °C right before heating for in situ study; and (c) in situ: initial dry gel mixed with 0.4 mL of additional water. The in situ spectrum was taken at 200 °C after heating for 15 h.

SDAs play a very important role in the assembly of molecular sieves by directing the formation of a specific structure during the synthesis.[106] In situ ^{13}C CP MAS NMR (Figure 6) was used to probe the behavior of the SDA in the $AlPO_4$-11 crystallization (i.e., crystallization at 200 °C using the dry gel sample with additional 0.4 mL of water). ^{1}H → ^{13}C CP intensity depends on the strength of the dipolar interaction between the proton and ^{13}C, which is modulated by the mobility of the molecule examined. As shown in Figure 6, the ^{1}H → ^{13}C CP MAS spectrum of the dry gel at 20 °C has three signals at 49.6, 19.9, and 11.8 ppm corresponding to the methylene carbon adjacent to nitrogen (C1), the second methylene carbon (C2), and the methyl carbon (C3) groups (Scheme S2 and Table S1) present in the protonated DPA (the SDA).[104] The appearance of the signals belonging to $DPAH^+$ ion at 20 °C implies that there is a strong interaction between the $DPAH^+$ with the inorganic species in the initial dry gel. The overall CP intensities of all three carbons increase when temperatures were raised to 50 and 80 °C, suggesting that the reorganization of dry gel structure at these temperatures leads to a local environment where the SDA is more rigid, hinting a stronger interaction between inorganic

https://doi.org/10.1021/jacsau.3c00109
JACS Au 2023, 3, 1670−1683

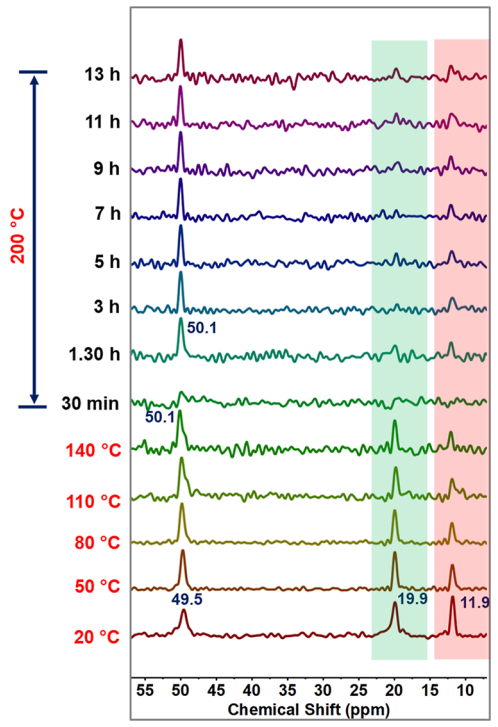

Figure 6. In situ $^{1}H \rightarrow {}^{13}C$ CP MAS NMR spectra of the dry gel samples (1.0 g) mixed with additional 0.4 mL of water. The spinning rate is 4.7 kHz.

and organic species. However, the overall CP intensities become rather poor as crystallization proceeds with further increasing temperature. The signals of the SDA almost completely disappear when 200 °C is reached. As discussed earlier, the protonated DPA ($DPAH^{+}$) in the initial dry gel becomes deprotonated as crystallization proceeds, and only DPA molecules are occluded inside the final $AlPO_4$-11. It appears that the DPA becomes highly mobile upon deprotonation. The ^{13}C NMR data are consistent with those of ^{1}H NMR. Beyond 200 °C, the intensity of the C1 carbon in the DPA is consistently stronger than the other two, implying that the amine end may experience restricted movements due to the hydrogen bonding with the AlPO species. Upon reaching the crystallization temperature, there is a very small but detectable change in the chemical shift of the C1 from 49.5 to 50.1 ppm, likely reflecting the deprotonation of the SDA.

Combining all the pieces of information obtained from in situ data in this study, as well as that from our previous ex situ DGC studies,[86,88,92] a formation pathway for $AlPO_4$-11 can be proposed: (1) upon drying the gel resulting from mixing DPA with Al and P sources together, solid amorphous materials were formed. This initial dry gel has one-dimensional aluminophosphate chains containing four- and six-membered rings, which are formed under the direction of protonated DPA. (2) The structures of the amorphous materials undergo reorganization as soon as the heating begins under DGC conditions. The transformation of the amorphous-to-crystalline two-dimensional layered phase begins immediately when the crystallization temperature is reached. It is noticed by in situ ^{1}H MAS NMR that during early heating, $DPAH^{+}$ becomes deprotonated. It is the neutral DPA molecules that play the structural directing role in the formation of a layered intermediate. (3) It appears that the formation of a 2D layered phase involves cross-linking the 1D chains with four- and six-membered rings into a 2D layered structure and occurs via Al−O−P bond breaking and formation. (4) The layers which have similar characteristics of the *ab* plan of the AEL structure stack together via hydrogen bonding to form a 3D structure that eventually evolves into crystalline $AlPO_4$-11, confirmed by the in situ $^{1}H \rightarrow {}^{31}P$ CP MAS NMR. This pathway is illustrated in Scheme 2. Similar formation pathways

Scheme 2. Schematic Representation of the Proposed Mechanism for Formation of the $AlPO_4$-11 Framework

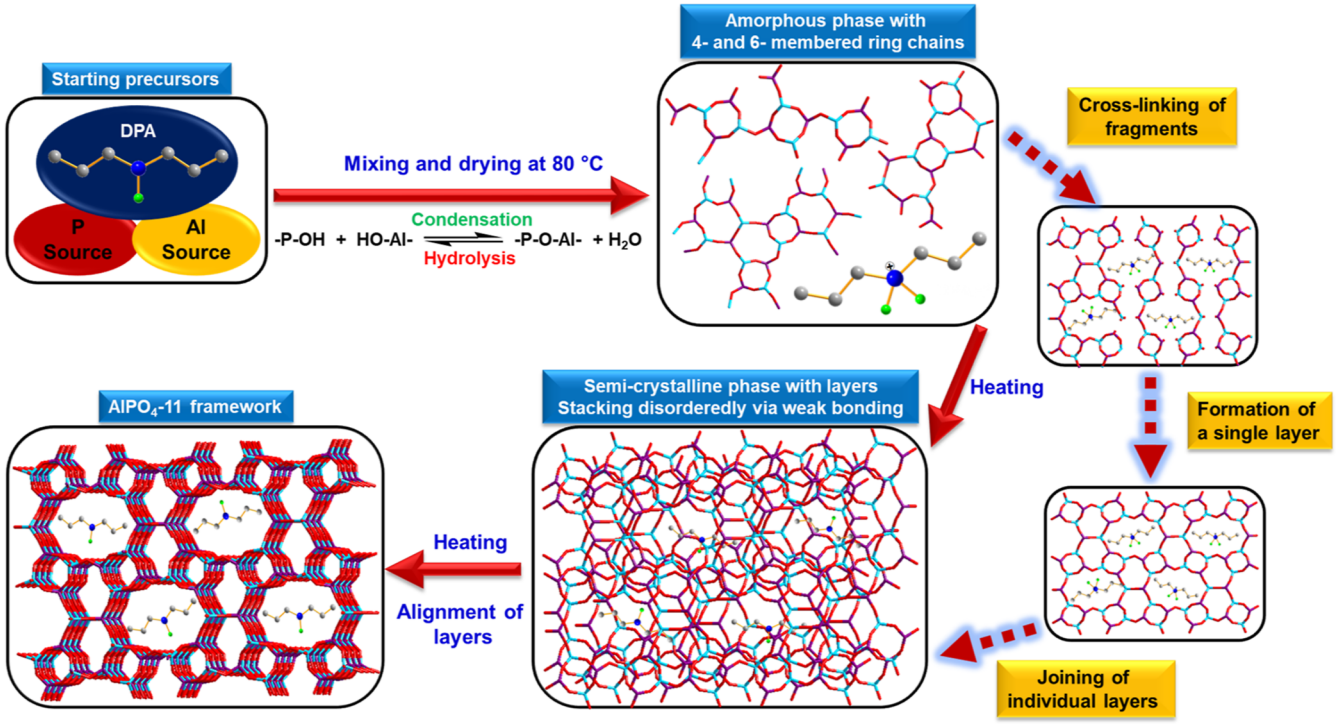

https://doi.org/10.1021/jacsau.3c00109
JACS Au 2023, 3, 1670−1683

under DGC conditions have been suggested in the literature,[85,86,90,92] but since they are all based on ex situ NMR studies, ambiguities do exist. The present comprehensive in situ multinuclear SSNMR study provides rich information on the evolution of the gel phases as a function of crystallization in real time and critical details at actual conditions (i.e., temperature and pressure) under which the crystallization occurs. The in situ study significantly reduces the ambiguities associated with ex situ, allowing us to refine the proposed model with confidence.

SUMMARY

The in situ multinuclear solid-state NMR spectroscopy has not only provided direct evidence on the speciation of the intermediates and structural units that are critical to the self-assembly of AEL topology but also revealed several key reactions/processes in detail, which are important in understanding the crystallization. Specifically, in situ ^{31}P MAS allows us to clearly monitor the integration of the tetrahedral Al and P fragments associated with four- and six-membered rings and other simple nutrients tethered on the solids into the layered materials and eventually into the $AlPO_4$-11 framework in real time. In situ ^{27}Al MAS NMR unambiguously demonstrates the transformation of the layered intermediate to $AlPO_4$-11. In situ $^{1}H \rightarrow {}^{31}P$ CP MAS spectra unveiled the details of how three inequivalent P sites in $AlPO_4$-11 are formed in the early stages of the crystallization, providing a concrete support for the proposed 2D → 3D formation mechanism. In situ ^{13}C CP MAS spectra furnish information on the mobility of the SDA, hence hydrogen bonding.

In situ ^{1}H MAS NMR was particularly fascinating. Because of the way the experiment was designed, high-resolution ^{1}H MAS spectra were obtained even at a low spinning speed of 4.7 kHz, allowing more information on the role of water to be extracted easily. An in situ ^{1}H MAS study indicates that under the DGC conditions used, the SDA exists as a neutral amine rather than in its protonated form in both the layered phase and $AlPO_4$-11. Apparently, under the DGC conditions, protonated DPA plays an important role in forming the initial dry gel containing 1D chains with four- and six-membered rings. It is the neutral amine that helps the transformation of the amorphous materials into the 2D layered phase where the DPA lies within each layer. The neutral DPA eventually was carried into the $AlPO_4$-11 structure upon layers' cross-linking to form a 3D covalent bonded AEL structure. It is apparent that forming different inorganic AlPO species, such as various 1D chains and 2D layered materials, requires slightly different hydrogen bonding with the SDA, which is provided by protonated and neutral DPA. In situ ^{1}H MAS NMR results also indicate that the water content in the initial dry gel is also important. When the water content is high enough, a small liquid phase can be formed in situ at crystallization temperature. This free/mobile water is needed to assist in Al−O−P bond breaking and reforming, facilitating crystallization. If the water content of the free water formed at crystallization temperature is too low, the SDA is immobile as indicated by the in situ NMR results. Consequently, the crystallization of $AlPO_4$-11 becomes very slow.

At this point, a few comments can be made on using in situ and ex situ solid-state NMR methods for examining the crystallization of molecular sieves. In situ multinuclear MAS NMR is a powerful method for examining molecular sieve formation by directly monitoring the evolution of the local environments of framework elements and the role of solvent and SDA in real time and at actual crystallization temperature and pressure. Some information, such as the role of water, the effect of water content on crystallization at the molecular level and the mobility of the SDA at high temperature and pressure is very difficult to obtain via ex situ studies. Additionally, in situ NMR allows one to follow the reactions in the stages before the crystallization temperature is reached. In situ data truly reflect what is happening at elevated temperature and pressure and are generally free of ambiguities encountered in ex situ studies caused by quenching reactions and altering the structures of intermediates by washing and drying solid materials during isolation/separation of solids from liquid.

However, there are some limitations of in situ studies. One such limitation is that the identification and characterization of some reactive and intermediate species often require using advanced solid-state NMR techniques, such as MQMAS, HETCOR, DQ-SQ, etc. These are 2D NMR methods, and many of them inherently have low sensitivity and low efficiency and therefore are time-consuming. Requiring a significant amount of time to get meaningful spectra presents a problem for in situ studies as the reactions can proceed significantly during data acquisition, yielding information averaged during the acquisition. On the other hand, the present work shows that if the ex situ studies were performed properly, the results are consistent with those obtained from the in situ study. Therefore, the best approach for examining the crystallization of molecular sieves is the combination of both ex situ and in situ NMR studies. An ex situ study should be carried out first as it allows one to identify the possible reactive intermediates and characterize them with various methods [PXRD, XAS using synchrotron radiation, vibrational (IR/Raman) spectroscopy, electron microscopy (SEM and TEM), and solid-state NMR]. In situ multinuclear MAS NMR will then be used to confirm and expand the results from the ex situ study and provide new information that is exclusively from the in situ study. Combing the ex situ and in situ results will provide a more clear, more comprehensive, and much less ambiguous picture of the formation of molecular sieves. The present work on the formation of $AlPO_4$-11 is a good example of application of such protocols.

ASSOCIATED CONTENT

Supporting Information

The Supporting Information is available free of charge at https://pubs.acs.org/doi/10.1021/jacsau.3c00109.

TGA profile; additional PXRD patterns; additional NMR data; structures of the SDA and its protonated form along with their ^{13}C and ^{1}H chemical shifts; and reaction vessel used for ex situ crystallization under the DGC condition (PDF)

AUTHOR INFORMATION

Corresponding Author

Yining Huang − *Department of Chemistry, The University of Western Ontario, London, Ontario N6A 5B7, Canada;* orcid.org/0000-0001-9265-5896; Email: yhuang@uwo.ca

https://doi.org/10.1021/jacsau.3c00109
JACS Au 2023, 3, 1670−1683

Authors

Sandamini H. Alahakoon − *Department of Chemistry, The University of Western Ontario, London, Ontario N6A 5B7, Canada*

Mathew J. Willans − *Department of Chemistry, The University of Western Ontario, London, Ontario N6A 5B7, Canada*

Complete contact information is available at: https://pubs.acs.org/10.1021/jacsau.3c00109

Author Contributions

CRediT: **Sandamini H Alahakoon** conceptualization, formal analysis, investigation, methodology, visualization, writing-original draft; **Mathew J. Willans** methodology, resources, writing-review & editing; **Yining Huang** conceptualization, formal analysis, funding acquisition, methodology, project administration, writing-review & editing.

Notes

The authors declare no competing financial interest.

■ ACKNOWLEDGMENTS

Y.H. thanks the Natural Science and Engineering Research Council (NSERC) of Canada for a Discovery Grant.

■ REFERENCES

(1) Corma, A. From Microporous to Mesoporous Molecular Sieve Materials and Their Use in Catalysis. *Chem. Rev.* **1997**, *97*, 2373−2420.

(2) Davis, M. E. Ordered Porous Materials for Emerging Applications. *Nature* **2002**, *417*, 813−821.

(3) Pool, R. The Smallest Chemical Plants: Zeolites-Crystalline Materials Riddled with Nanometer-Sized Cavities-Can Exert Exquisite Control over Chemical Reactions and Produce Devices on the Smallest Scale. *Science* **1994**, *263*, 1698−1699.

(4) Cundy, C. S.; Cox, P. A. The Hydrothermal Synthesis of Zeolites: History and Development from the Earliest Days to the Present Time. *Chem. Rev.* **2003**, *34*, 663.

(5) Wilson, S. T.; Lok, B. M.; Messina, C. A.; Cannan, T. R.; Flanigen, E. M. Aluminophosphate Molecular Sieves: A New Class of Microporous Crystalline Inorganic Solids. *J. Am. Chem. Soc.* **1982**, *104*, 1146−1147.

(6) Potter, M. E. Down the Microporous Rabbit Hole of Silicoaluminophosphates: Recent Developments on Synthesis, Characterization, and Catalytic Applications. *ACS Catal.* **2020**, *10*, 9758−9789.

(7) Yu, J.; Xu, R. Insight into the Construction of Open-Framework Aluminophosphates. *Chem. Soc. Rev.* **2006**, *37*, 593.

(8) Hartmann, M.; Kevan, L. Transition-Metal Ions in Aluminophosphate and Silicoaluminophosphate Molecular Sieves: Location, Interaction with Adsorbates and Catalytic Properties. *Chem. Rev.* **1999**, *99*, 635.

(9) Davis, M. E.; Lobo, R. F. Zeolite and Molecular Sieve Synthesis. *Chem. Mater.* **1992**, *4*, 756−768.

(10) Li, J.; Yu, J.; Xu, R. Progress in Heteroatom-Containing Aluminophosphate Molecular Sieves. *Proc. R. Soc. A* **2012**, *468*, 1955−1967.

(11) Cundy, C. S.; Cox, P. A. The Hydrothermal Synthesis of Zeolites: Precursors, Intermediates and Reaction Mechanism. *Microporous Mesoporous Mater.* **2005**, *82*, 1−78.

(12) Cheetham, A. K.; Fe, Â.; Loiseau, T. New Materials Try to Emulate Nature s Open Frameworks. *Angew. Chem., Int. Ed.* **1999**, *38*, 3269.

(13) Francis, R. J.; O'Hare, D.; Francis, R. J.; Hare, D. O. The Kinetics and Mechanisms of the Crystallisation of Microporous Materials. *J. Chem. Soc., Dalton Trans.* **1998**, *19*, 3133−3148.

(14) Jones, C. W.; Hwang, S. J.; Okubo, T.; Davis, M. E. Synthesis of Hydrophobic Molecular Sieves by Hydrothermal Treatment with Acetic Acid. *Chem. Mater.* **2001**, *13*, 1041−1050.

(15) Epping, J. D.; Chmelka, B. F. Nucleation and Growth of Zeolites and Inorganic Mesoporous Solids: Molecular Insights from Magnetic Resonance Spectroscopy. *Curr. Opin. Colloid Interface Sci.* **2006**, *11*, 81−117.

(16) Francis, R. J.; O'Hare, D. The Kinetics and Mechanisms of the Crystallisation of Microporous Materials. *J. Chem. Soc., Dalton Trans.* **1998**, *7*, 3133−3148.

(17) Haouas, M. Nuclear Magnetic Resonance Spectroscopy for *In Situ* Monitoring of Porous Materials Formation under Hydrothermal Conditions. *Materials* **2018**, *11*, 1416.

(18) Xu, W.; Dong, J.; Li, J.; Li, J.; Wu, F. A Novel Method for the Preparation of Zeolite ZSM-5. *J. Chem. Soc., Chem. Commun.* **1990**, *755*, 755.

(19) Bandyopadhyay, M.; Bandyopadhyay, R.; Kubota, Y.; Sugi, Y. Synthesis of $AlPO_4$-5 and $AlPO_4$-11 Molecular Sieves by Dry-Gel Conversion Method. *Chem. Lett.* **2000**, *29*, 1024−1025.

(20) Bandyopadhyay, R.; Bandyopadhyay, M.; Kubota, Y.; Sugi, Y. Synthesis of $AlPO_4$ Molecular Sieves with AFI and AEL Structures by Dry-Gel Conversion Method and Catalytic Application of Their SAPO Counterparts on Isopropylation of Biphenyl. *J. Porous Mater.* **2002**, *9*, 83−95.

(21) Rao, P. R. H. P.; Matsukata, M. Dry-Gel Conversion Technique for Synthesis of Zeolite BEA. *Chem. Commun.* **1996**, *2*, 1441.

(22) Sheng, N.; Chu, Y.; Xin, S.; Wang, Q.; Yi, X.; Feng, Z.; Meng, X.; Liu, X.; Deng, F.; Xiao, F. S. Insights of the Crystallization Process of Molecular Sieve $AlPO_4$-5 Prepared by Solvent-Free Synthesis. *J. Am. Chem. Soc.* **2016**, *138*, 6171−6176.

(23) Zhou, D.; Lu, X.; Xu, J.; Yu, A.; Li, J.; Deng, F.; Xia, Q. Dry Gel Conversion Method for the Synthesis of Organic-Inorganic Hybrid MOR Zeolites with Modifiable Catalytic Activities. *Chem. Mater.* **2012**, *24*, 4160−4165.

(24) Goergen, S.; Guillon, E.; Patarin, J.; Rouleau, L. Shape Controlled Zeolite EU-1 (EUO) Catalysts: Dry Gel Conversion Type Synthesis, Characterization and Formation Mechanisms. *Microporous Mesoporous Mater.* **2009**, *126*, 283−290.

(25) Wu, Q.; Meng, X.; Gao, X.; Xiao, F. S. Solvent-Free Synthesis of Zeolites: Mechanism and Utility. *Acc. Chem. Res.* **2018**, *51*, 1396−1403.

(26) Chen, B.; Huang, Y. Formation of Microporous Material $AlPO_4$-18 under Dry-Gel Conversion Conditions. *Microporous Mesoporous Mater.* **2011**, *143*, 14−21.

(27) Chen, B.; Kirby, C. W.; Huang, Y. Investigation of Crystallization of Molecular Sieve $AlPO_4$-5 by the Dry Gel Conversion Method. *J. Phys. Chem. C* **2009**, *113*, 15868−15876.

(28) Xu, J.; Chen, L.; Zeng, D.; Yang, J.; Zhang, M.; Ye, C.; Deng, F. Crystallization of $AlPO_4$-5 Aluminophosphate Molecular Sieve Prepared in Fluoride Medium: A Multinuclear Solid-State NMR Study. *J. Phys. Chem. B* **2007**, *111*, 7105−7113.

(29) Kim, M. H.; Li, H. X.; Davis, M. E. Synthesis of Zeolites by Water-Organic Vapor-Phase Transport. *Microporous Mater.* **1993**, *1*, 191−200.

(30) Ren, L.; Li, C.; Fan, F.; Guo, Q.; Liang, D.; Feng, Z.; Li, C.; Li, S.; Xiao, F. S. UV-Raman and NMR Spectroscopic Studies on the Crystallization of Zeolite A and a New Synthetic Route. *Chem.—Eur. J.* **2011**, *17*, 6162−6169.

(31) Matsukata, M.; Ogura, M.; Osaki, T.; Hari Prasad Rao, P. R.; Nomura, M.; Kikuchi, E. Conversion of Dry Gel to Microporous Crystals in Gas Phase. *Top. Catal.* **1999**, *9*, 77−92.

(32) Kumar, M.; Choudhary, M. K.; Rimer, J. D. Transient Modes of Zeolite Surface Growth from 3D Gel-like Islands to 2D Single Layers. *Nat. Commun.* **2018**, *9*, 2129.

(33) Van Vleet, M. J.; Weng, T.; Li, X.; Schmidt, J. R. *In Situ*, Time-Resolved, and Mechanistic Studies of Metal-Organic Framework Nucleation and Growth. *Chem. Rev.* **2018**, *118*, 3681−3721.

(34) Férey, G.; Haouas, M.; Loiseau, T.; Taulelle, F. Nanoporous Solids: How Do They Form? An *In Situ* Approach. *Chem. Mater.* **2014**, *26*, 299−309.
(35) Norby, P. Hydrothermal Conversion of Zeolites: An *In Situ* Synchrotron X-Ray Powder Diffraction Study. *J. Am. Chem. Soc.* **1997**, *119*, 5215−5221.
(36) Norby, P.; Hanson, J. C. Hydrothermal Synthesis of the Microporous Aluminophosphate CoAPO-5; *In Situ* Time-Resolved Synchrotron X-Ray Powder Diffraction Studies. *Catal. Today* **1998**, *39*, 301−309.
(37) Norby, P. In-Situ XRD as a Tool to Understanding Zeolite Crystallization. *Curr. Opin. Colloid Interface Sci.* **2006**, *11*, 118−125.
(38) Sankar, G.; Okubo, T.; Fan, W.; Meneau, F. New Insights into the Formation of Microporous Materials by *In Situ* Scattering Techniques. *Faraday Discuss.* **2007**, *136*, 157.
(39) O'Brien, M. G.; Beale, A. M.; Kuipers, B. W. M.; Erné, B. H.; Lewis, D. W.; Catlow, C. R. A. Role of Germanium on the Nucleation and Growth of Zeolite a from Clear Solutions as Studied by *In Situ* Small-Angle X-Ray Scattering, Wide-Angle X-Ray Scattering, and Dynamic Light Scattering. *J. Phys. Chem. C* **2009**, *113*, 18614−18622.
(40) Fan, W.; Ogura, M.; Sankar, G.; Okubo, T. In situ Small-Angle and Wide-Angle X-ray Scattering Investigation on Nucleation and Crystal Growth of Nanosized Zeolite A. *Chem. Mater.* **2007**, *19*, 1906−1917.
(41) Fengtao, F.; Zhaochi, F.; Can, L. UV Raman Spectroscopic Study on the Synthesis Mechanism and Assembly of Molecular Sieves. *Chem. Soc. Rev.* **2010**, *39*, 4794−4801.
(42) Fan, F.; Feng, Z.; Sun, K.; Guo, M.; Guo, Q.; Song, Y.; Li, W.; Li, C. *In Situ* UV Raman Spectroscopic Study on the Synthesis Mechanism of AlPO-5. *Angew. Chem., Int. Ed.* **2009**, *48*, 8743−8747.
(43) Groen, J. C.; Hamminga, G. M.; Moulijn, J. A.; Pérez-Ramírez, J. *In Situ* Monitoring of Desilication of MFI-Type Zeolites in Alkaline Medium. *Phys. Chem. Chem. Phys.* **2007**, *9*, 4822.
(44) Choudhary, M. K.; Jain, R.; Rimer, J. D. *In Situ* Imaging of Two-Dimensional Surface Growth Reveals the Prevalence and Role of Defects in Zeolite Crystallization. *Proc. Natl. Acad. Sci. U.S.A.* **2020**, *117*, 28632−28639.
(45) Linares, N.; Sachse, A.; Serrano, E.; Grau-Atienza, A.; De Oliveira Jardim, E.; Silvestre-Albero, J.; Cordeiro, M. A. L.; Fauth, F.; Beobide, G.; Castillo, O.; García-Martínez, J. *In Situ* Time-Resolved Observation of the Development of Intracrystalline Mesoporosity in USY Zeolite. *Chem. Mater.* **2016**, *28*, 8971−8979.
(46) Itzel Meza, L.; Anderson, M. W.; Slater, B.; Agger, J. R. *In Situ* Atomic Force Microscopy of Zeolite A Dissolution. *Phys. Chem. Chem. Phys.* **2008**, *10*, 5066.
(47) Ashbrook, S. E.; Dawson, D. M.; Seymour, V. R. Recent Developments in Solid-State NMR Spectroscopy of Crystalline Microporous Materials. *Phys. Chem. Chem. Phys.* **2014**, *16*, 8223−8242.
(48) Christopher Roe, D. Sapphire NMR Tube for High-Resolution Studies at Elevated Pressure. *J. Magn. Reson.* **1985**, *63*, 388−391.
(49) Kinrade, S. D.; Swaddle, T. W. A Sample Tube for Nmr Studies at Elevated Pressures and Temperatures. *J. Magn. Reson.* **1988**, *77*, 569−571.
(50) Jouanne, J. V.; Heidberg, J. High Resolution NMR under Increased Hydrostatic Pressure: Keto-Enol Equilibrium of Acetylacetone. *J. Magn. Reson.* **1972**, *7*, 1−4.
(51) Bai, S.; Taylor, C. M.; Mayne, C. L.; Pugmire, R. J.; Grant, D. M. A New High Pressure Sapphire Nuclear Magnetic Resonance Cell. *Rev. Sci. Instrum.* **1996**, *67*, 240−243.
(52) Horváth, I. T.; Ponce, E. C. New Valve Design for High-pressure Sapphire Tubes for NMR Measurements. *Rev. Sci. Instrum.* **1991**, *62*, 1104−1105.
(53) Yamada, H. Pressure-resisting Glass Cell for High Pressure, High Resolution NMR Measurement. *Rev. Sci. Instrum.* **1974**, *45*, 640−642.
(54) Gerardin, C.; Haouas, M.; Lorentz, C.; Taulelle, F. NMR Quantification in Hydrothermal *In Situ* Syntheses. *Magn. Reson. Chem.* **2000**, *38*, 429−435.
(55) Taulelle, F.; Haouas, M.; Gerardin, C.; Estournes, C.; Loiseau, T.; Ferey, G. NMR of microporous compounds: From in situ reactions to solid paving. *Colloids Surf., A* **1999**, *158*, 299−311.
(56) Haouas, M.; Gerardin, C.; Taulelle, F.; Estournes, C.; Loiseau, T.; Ferey, G. *In Situ* NMR Study of Hydrothermal Synthesis of a Template-Mediated Microporous Aluminophosphate Material: $AlPO_4$-CJ2. *J. Chim. Phys. Phys.-Chim. Biol.* **1998**, *95*, 302−309.
(57) Vistad, Ø. B.; Akporiaye, D. E.; Taulelle, F.; Lillerud, K. P. *In Situ* NMR of SAPO-34 Crystallization. *Chem. Mater.* **2003**, *34*, 1639.
(58) Miladinović, Z.; Zakrzewska, J.; Kovačević, B.; Bačić, G. Monitoring of Crystallization Processes during Synthesis of Zeolite A by *In Situ* ^{27}Al NMR Spectroscopy. *Mater. Chem. Phys.* **2007**, *104*, 384−389.
(59) In-Gérardin, C.; In, M.; Taulelle, F.; Taulelle, F. *In Situ* NMR Measurements under Hydrothermal Conditions: Study of the Formation of Polymeric Al Hydrolysis Species. *J. Chim. Phys.* **1995**, *92*, 1877−1880.
(60) Serre, C.; Lorentz, C.; Taulelle, F.; Férey, G. Hydrothermal Synthesis of Nanoporous Metalofluorophosphates. 2. *In Situ* and *Ex Situ* ^{19}F and ^{31}P NMR of Nano- and Mesostructured Titanium Phosphates Crystallogenesis. *Chem. Mater.* **2003**, *15*, 2328−2337.
(61) Xu, J.; Liu, Y.; Huang, Y. Ultrafast Crystallization of $AlPO_4$-5 Molecular Sieve in a Deep Eutectic Solvent. *J. Phys. Chem. C* **2021**, *125*, 8876−8889.
(62) Shi, J.; Anderson, M. W.; Carr, S. W. Direct Observation of Zeolite a Synthesis by *In Situ* Solid-State NMR. *Chem. Mater.* **1996**, *8*, 369−375.
(63) Maistriau, L.; Gabelica, Z.; Derouane, E. G. Dehydration of (DPA) VPI-5: *In Situ* Variable Temperature Multinuclear NMR Investigations. *Appl. Catal., A* **1992**, *81*, 67−80.
(64) Akporiaye, D.; Stöcker, M. *In Situ* Variable-Temperature Solid-State NMR Study of VPI-5 and $AlPO_4$-8 at Different Degrees of Transformation. *Microporous Mater.* **1993**, *1*, 431−435.
(65) Akporiaye, D.; Stöcker, M. Solid-State n.m.r. and XRD Study of the Thermal Stability of VPI-5: Assignment of ^{31}P and ^{27}AI MAS n.m.r. Spectra. *Zeolites* **1992**, *12*, 351−359.
(66) Romanova, E. E.; Scheffler, F.; Freude, D. Crystallization of Zeolite MFI under Supergravity, Studied *In Situ* by ^{11}B MAS NMR Spectroscopy. *Microporous Mesoporous Mater.* **2009**, *126*, 268−271.
(67) Deuchande, T.; Breton, O.; Haedelt, J.; Hughes, E. Design and Performance of a High Pressure Insert for Use in a Standard Magic Angle Spinning NMR Probe. *J. Magn. Reson.* **2006**, *183*, 178−182.
(68) Hu, J. Z.; Hu, M. Y.; Zhao, Z.; Xu, S.; Vjunov, A.; Shi, H.; Camaioni, D. M.; Peden, C. H. F.; Lercher, J. A. Sealed Rotors for *In Situ* High Temperature High Pressure MAS NMR. *Chem. Commun.* **2015**, *51*, 13458−13461.
(69) Ivanova, I. I.; Kolyagin, Y. G.; Kasyanov, I. A.; Yakimov, A. V.; Bok, T. O.; Zarubin, D. N. Time-Resolved *In Situ* MAS NMR Monitoring of the Nucleation and Growth of Zeolite BEA Catalysts under Hydrothermal Conditions. *Angew. Chem., Int. Ed.* **2017**, *56*, 15344−15347.
(70) Ivanova, I. I.; Kolyagin, Y. G. Application of Multinuclear MAS NMR for the *In Situ* Monitoring of Hydrothermal Synthesis of Zeolites. *Chem.—Eur. J.* **2021**, *27*, 14143−14167.
(71) Aerts, A.; Kirschhock, C. E. A.; Martens, J. A. Methods for *In Situ* Spectroscopic Probing of the Synthesis of a Zeolite. *Chem. Soc. Rev.* **2010**, *39*, 4626.
(72) Ivanova, I. I.; Kolyagin, Y. G. Impact of *In Situ* MAS NMR Techniques to the Understanding of the Mechanisms of Zeolite Catalyzed Reactions. *Chem. Soc. Rev.* **2010**, *39*, 5018.
(73) Cheetham, A. K.; Mellot, C. F. *In Situ* Studies of the Sol-Gel Synthesis of Materials. *Chem. Mater.* **1997**, *9*, 2269−2279.
(74) Broom, L. K.; Clarkson, G. J.; Guillou, N.; Hooper, J. E.; Dawson, D. M.; Tang, C. C.; Ashbrook, S. E.; Walton, R. I. A Gel Aging Effect in the Synthesis of Open-Framework Gallium Phosphates: Structure Solution and Solid-State NMR of a Large-Pore, Open-Framework Material. *Dalton Trans.* **2017**, *46*, 16895−16904.

https://doi.org/10.1021/jacsau.3c00109
JACS Au 2023, 3, 1670−1683

(75) Morris, S. A.; Bignami, G. P. M.; Tian, Y.; Navarro, M.; Firth, D. S.; Cejka, J.; Wheatley, P. S.; Dawson, D. M.; Slawinski, W. A.; Wragg, D. S.; Morris, R. E.; Ashbrook, S. E. *In Situ* Solid-State NMR and XRD Studies of the ADOR Process and the Unusual Structure of Zeolite IPC-6. *Nat. Chem.* **2017**, *9*, 1012−1018.
(76) Paula, C.; Wisser, D.; Rangus, M.; Schwieger, W.; Hovestadt, M.; Kriesten, M.; Vanatalu, K.; Oss, A.; Org, M. L.; Samoson, A.; Hartmann, M. Phase Transformations in Porous Materials Studied by *In Situ* Solid-State NMR Spectroscopy and in Situ X-Ray Diffraction. *J. Phys. Chem. C* **2020**, *124*, 19136−19145.
(77) Zhao, Z.; Xu, S.; Hu, M. Y.; Bao, X.; Hu, J. Z. *In Situ* High Temperature High Pressure MAS NMR Study on the Crystallization of $AlPO_4$-5. *J. Phys. Chem. C* **2016**, *120*, 1701−1708.
(78) Ashbrook, S. E.; Morris, R.; Rice, C. M. Understanding the Synthesis and Reactivity of ADORable Zeolites Using NMR Spectroscopy. *Curr. Opin. Colloid Interface Sci.* **2022**, *61*, 101634.
(79) Bennett, J. M.; Richardson, J. W.; Pluth, J. J.; Smith, J. V. Aluminophosphate Molecular Sieve $AlPO_4$-11: Partial Refinement from Powder Data Using a Pulsed Neutron Source. *Zeolites* **1987**, *7*, 160−162.
(80) Khemaissia, S.; Nibou, D.; Amokrane, S.; Lebaili, N. Use of AlPO-11, SnAPO-11, SAPO-31 and SAPO-41 Elaborated Solid Materials as Catalysts in Ammonia Alkylation Reaction. *J. Appl. Sci.* **2007**, *7*, 2371−2375.
(81) Springuel-Huet, M. A.; Fraissard, J. 129Xe NMR of Xenon Adsorbed on the Molecular Sieves $AlPO_4$-11 and SAPO-11. Chemical Shift Anisotropy Related to the Asymmetry of the Adsorption Zones. *Chem. Phys. Lett.* **1989**, *154*, 299−302.
(82) Prakash, A. M.; Chilukuri, S. V. V.; Bagwe, R. P.; Ashtekar, S.; Chakrabarty, D. K. Silicoaluminophosphate Molecular Sieves SAPO-11, SAPO-31 and SAPO-41: Synthesis, Characterization and Alkylation of Toluene with Methanol. *Microporous Mater.* **1996**, *6*, 89−97.
(83) Martens, J. A.; Grobet, P. J.; Jacobs, P. A. Catalytic Activity and Si, Al, P Ordering in Microporous Silicoaluminophosphates of the SAPO-5, SAPO-11, and SAPO-37 Type. *J. Catal.* **1990**, *126*, 299−305.
(84) Zhang, B.; Xu, J.; Fan, F.; Guo, Q.; Tong, X.; Yan, W.; Yu, J.; Deng, F.; Li, C.; Xu, R. Molecular Engineering of Microporous Crystals: (III) the Influence of Water Content on the Crystallization of Microporous Aluminophosphate $AlPO_4$-11. *Microporous Mesoporous Mater.* **2012**, *147*, 212−221.
(85) Cheng, T.; Xu, J.; Li, X.; Li, Y.; Zhang, B.; Yan, W.; Yu, J.; Sun, H.; Deng, F.; Xu, R. Molecular Engineering of Microporous Crystals: (IV) Crystallization Process of Microporous Aluminophosphate $AlPO_4$-11. *Microporous Mesoporous Mater.* **2012**, *152*, 190−207.
(86) Chen, B.; Huang, Y. Examining the Self-Assembly of Microporous Material $AlPO_4$-11 by Dry-Gel Conversion. *J. Phys. Chem. C* **2007**, *111*, 15236−15243.
(87) Xu, R.; Zhang, W.; Xu, J.; Tian, Z.; Deng, F.; Han, X.; Bao, X. Multinuclear Solid-State NMR Studies on the Formation Mechanism of Aluminophosphate Molecular Sieves in Ionic Liquids. *J. Phys. Chem. C* **2013**, *117*, 5848−5854.
(88) Chen, B.; Huang, Y. ^{17}O Solid-State NMR Spectroscopic Studies of the Involvement of Water Vapor in Molecular Sieve Formation by Dry-Gel Conversion. *J. Am. Chem. Soc.* **2006**, *128*, 6437−6446.
(89) Han, B.; Shin, C. H.; Cox, P. A.; Hong, S. B. Molecular Conformations of Protonated Dipropylamine in $AlPO_4$-11, $AlPO_4$-31, SAPO-34, and $AlPO_4$-41 Molecular Sieves. *J. Phys. Chem. B* **2006**, *110*, 8188−8193.
(90) Sheng, N.; Chu, Y.; Xin, S.; Wang, Q.; Liu, X.; Xu, J.; Xiao, F. S.; Deng, F. New Insights into the Di-n-Propylamine (DPA) Molecule as an Organic Structural Directing Agent (OSDA) in the Crystallization of $AlPO_4$-11 Molecular Sieve. *Inorg. Chem. Front.* **2018**, *5*, 1633−1639.
(91) Harris, K. D. M.; Hughes, C. E.; Williams, P. A.; Edwards-Gau, G. R. NMR Crystallization": *In-Situ* NMR Techniques for Time-Resolved Monitoring of Crystallization Processes. *Acta Crystallogr. C Struct. Chem.* **2017**, *73*, 137−148.
(92) Huang, Y.; Richer, R.; Kirby, C. W. Characterization of the Gel Phases of $AlPO_4$-11 Molecular Sieve Synthesis by Solid-State NMR. *J. Phys. Chem. B* **2003**, *107*, 1326−1337.
(93) Hartmann, S. R.; Hahn, E. L. Nuclear Double Resonance in the Rotating Frame. *Phys. Rev.* **1962**, *128*, 2042−2053.
(94) Blackwell, C. S.; Patton, R. L. Aluminum-27 and Phosphorus-31 Nuclear Magnetic Resonance Studies of Aluminophosphate Molecular Sieves. *J. Phys. Chem.* **1984**, *88*, 6135−6139.
(95) Blackwell, C. S.; Patton, R. L. Solid-State NMR of Silicoaluminophosphate Molecular Sieves and Aluminophosphate Materials. *J. Phys. Chem.* **1988**, *92*, 3965−3970.
(96) Mortlock, R. F.; Bell, A. T.; Radke, C. J. ^{31}P and $^{27}A1$ NMR Investigations of the Effects of pH on Aqueous Solutions Containing Aluminum and Phosphorus. *J. Phys. Chem.* **1993**, *97*, 775−782.
(97) Zhang, L.; Huang, Y. New Insights into Formation of Molecular Sieve SAPO-34 for MTO Reactions. *J. Phys. Chem. C* **2016**, *120*, 25945−25957.
(98) Longstaffe, J. G.; Chen, B.; Huang, Y. Characterization of the Amorphous Phases Formed during the Synthesis of Microporous Material $AlPO_4$-5. *Microporous Mesoporous Mater.* **2007**, *98*, 21−28.
(99) Zhang, L.; Chen, D.; Nie, H.-Y.; Huang, Y. A Study of the Formation of Microporous Material SAPO-37. *Microporous Mesoporous Mater.* **2013**, *175*, 147−156.
(100) Meriaudeau, P.; Tuan, V. A.; Nghiem, V. T.; Lai, S. Y.; Hung, L. N.; Naccache, C. SAPO-11, SAPO-31, and SAPO-41 Molecular Sieves: Synthesis, Characterization, and Catalytic Properties Inn-Octane Hydroisomerization. *J. Catal.* **1997**, *169*, 55−66.
(101) Huang, Y.; Demko, B. A.; Kirby, C. W. Investigation of the Evolution of Intermediate Phases of $AlPO_4$-18 Molecular Sieve Synthesis. *Chem. Mater.* **2003**, *15*, 2437−2444.
(102) MacIntosh, A. R.; Huang, Y. Formation of and Silicon Incorporation in SAPO-5 Synthesized via Dry-Gel Conversion. *Microporous Mesoporous Mater.* **2013**, *182*, 40−49.
(103) Barrie, P. J.; Smith, M. E.; Klinowski, J. Double-Rotation 27Al NMR Studies of the Aluminophosphate Molecular Sieve $AlPO_4$-11. *Chem. Phys. Lett.* **1991**, *180*, 6−12.
(104) Fan, D.; Tian, P.; Xu, S.; Wang, D.; Yang, Y.; Li, J.; Wang, Q.; Yang, M.; Liu, Z. SAPO-34 Templated by Dipropylamine and Diisopropylamine: Synthesis and Catalytic Performance in the Methanol to Olefin (MTO) Reaction. *New J. Chem.* **2016**, *40*, 4236−4244.
(105) Schneider, W. G.; Bernstein, H. J.; Pople, J. A. Proton Magnetic Resonance Chemical Shift of Free (Gaseous) and Associated (Liquid) Hydride Molecules. *J. Chem. Phys.* **1958**, *28*, 601−607.
(106) Xu, R.; Pang, W.; Yu, J.; Huo, Q.; Chen, J. *Chemistry of Zeolites and Related Porous Materials: Synthesis and Structure*; John Wiley & Sons (Asia) Pte Ltd.: Singapore, 2007.

https://doi.org/10.1021/jacsau.3c00109
JACS Au 2023, 3, 1670−1683